International Journal of Nanomedicine

Dovepress
Taylor & Francis Group

Open Access Full Text Article

ORIGINAL RESEARCH

Evaluation of *Artemisia annua-Scutellaria baicalensis* Herb Pair Carbon Dots Interfering NLRP3 Inflammatory Pathway For Effective Against H1N1 Viral Pneumonia in Mice Model

Qianyun Zhang[1,*], Xinyi Huang[1,*], Huimei Kong[2], Qiongyao Liang[1], Xiaoqing Lv[2], Yuan Ma[1], Jingbo Wang[3], Jing Chen[1]

[1]College of Life Science, Zhejiang Chinese Medical University, Hangzhou, People's Republic of China; [2]College of Life Science, Jinhua University of Vocational Technology, Jinhua, People's Republic of China; [3]Library, Zhejiang Chinese Medical University, Hangzhou, People's Republic of China

*These authors contributed equally to this work

Correspondence: Jing Chen, College of Life Science, Zhejiang Chinese Medicine University, No. 548, Binwen Road, Binjiang District, Hangzhou, Zhejiang, People's Republic of China, Tel +86613600, Fax +0571-86613712, Email cj00123@zcmu.edn.cn; Jingbo Wang, Library, Zhejiang Chinese Medicine University, No. 548, Binwen Road, Binjiang District, Hangzhou, Zhejiang, People's Republic of China, Tel +86613586, Fax +0571-86613586, Email yankee1997@126.com

Purpose: Influenza is an acute respiratory infectious disease with high transmissibility and significant pandemic potential worldwide. In recent years, traditional Chinese medicine (TCM)-based carbon dots (CDs) have emerged as promising therapeutic agents owing to their favorable biosafety profile and potent anti-inflammatory and immunomodulatory properties. The present study aimed to investigate the therapeutic effects of TCM-derived CDs on influenza A virus (IAV)-induced pneumonia, and elucidate their underlying molecular mechanisms of action.

Mouse Model and Methods: A murine model of IAV-induced pneumonia was established via intranasal instillation and subsequently treated with CDs co-derived from Artemisia annua and Scutellaria baicalensis (QH-CDs).

Results: The results demonstrated that, compared to the observations in the model group, treatment with QH-CDs significantly alleviated the pathological damages to lung tissue, reduced the lung index, and promoted body weight recovery. QH-CDs treatment reduced the expression of key inflammatory cytokines (IL-1β, IL-6) in lung tissue by over 60% compared to the model group ($p < 0.0001$). In addition, QH-CDs reduce lung viral titers by more than 70%, indicating that they have combined antiviral and anti-inflammatory effects. Transcriptomic analysis revealed that treatment with QH-CDs reversed the alterations in the expression patterns of several genes associated with immunity and inflammation. The differentially expressed genes were predominantly involved in immune regulation, cytokine activity, and inflammatory signaling pathways. The results of Quantitative Real-time polymerase chain reaction (qPCR) show that the mRNA expression levels of NLRP3, Caspase-1, and IL-1β all significantly decreased. Protein expression analyses by Western blotting further confirmed the critical role of the NLRP3 inflammasome signaling pathway in mediating the therapeutic effects of QH-CDs.

Conclusion: QH-CDs therapeutic effects may be closely related to the regulation of immune responses, inhibition of inflammatory responses, and modulation of the NLRP3 signaling pathway. This study provides novel insights into the therapeutic application of TCM-derived nanomaterials for the treatment of viral pneumonia.

Keywords: influenza A virus, carbon dots, NLRP3, *Artemisia annua*, *Scutellaria baicalensis*, traditional Chinese medicine, pneumonia

Introduction

Influenza is an acute respiratory infectious disease caused by influenza viruses and is characterized by high transmissibility and substantial morbidity. The World Health Organization estimates that influenza infects approximately 10% of the global

https://doi.org/10.2147/IJN.S566658
Received: 3 October 2025
Accepted: 10 January 2026
Published: 23 January 2026

Graphical Abstract

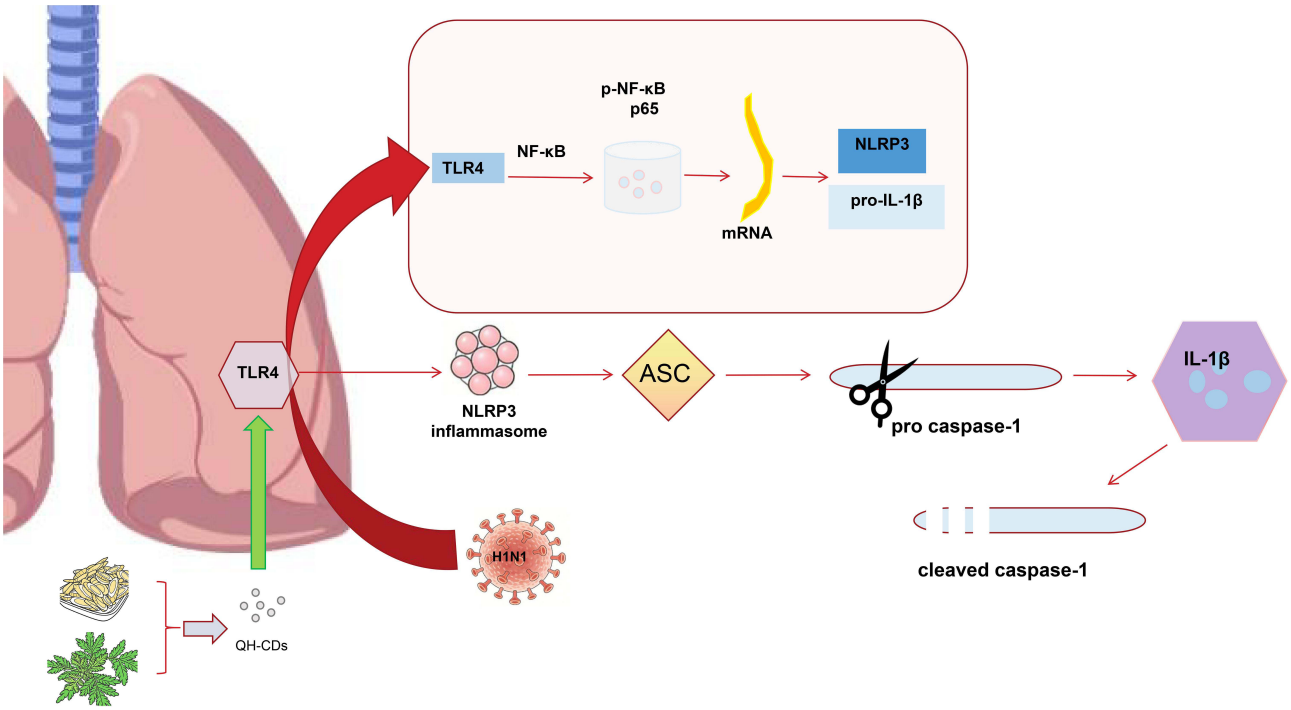

population annually, leading to 290,000–650,000 respiratory-related deaths worldwide.[1] Influenza A viruses (IAVs) have caused multiple global pandemics since the early 20th century and remain the dominant drivers of seasonal influenza epidemics, including in China, where influenza continues to show high incidence and recurrent outbreaks.[2] Influenza viruses exhibit multiple modes of transmission, including both interhuman and zoonotic routes, which facilitate their continued spread within populations. Therefore, the prevention and treatment of influenza have important implications for global public health. Due to their extremely high genetic variability, infections caused by IAVs can lead to numerous complications, among which viral pneumonia is one of the most common, characterized by wheezing, fever, and increased respiratory rate.[3] Viral pneumonia is also a major cause of mortality, thereby emphasizing the urgent need for developing antiviral therapies targeting IAV-induced pneumonia. At present, the preventative and therapeutic potential of influenza vaccines remains limited, making antiviral drugs an effective strategy for the control of influenza virus infections. Small molecule antivirals frequently employed in the targeted treatment of influenza infections include M2 ion channel blockers such as amantadine;[4] neuraminidase inhibitors such as oseltamivir;[5] and enzyme inhibitors such as mabaloxavir.[6] These drugs exhibit a broad spectrum of activity and a rapid onset of action; however, they are often associated with significant toxicities, adverse effects, and a high risk of allergic reactions. Additionally, the emergence of several drug-resistant influenza strains further restricts the therapeutic efficacy of existing antiviral agents. In recent years, several anti-influenza drugs targeting novel viral targets have emerged, including favipiravir;[7] however, their long-term efficacy remains uncertain. Therefore, there is an urgent necessity for developing novel, highly effective anti-influenza drugs that are safe, effective, and exert minimal adverse effects. The transition from single-target therapies in Western medicine to the multi-target and holistic approach of traditional Chinese medicine (TCM) not only complements existing treatment strategies but also represents a promising direction for future research and the development of novel anti-influenza drugs. TCM has a long-standing history in the prevention and treatment of respiratory tract infections in China, and numerous clinical studies have demonstrated that TCM prescriptions offer unique advantages in the prevention and treatment of influenza and COVID-19 infections. TCM has several advantages,

including reliable clinical efficacy, minimal adverse effects, low rates of drug resistance, and others. The majority of TCM prescriptions are plant-based, rich in medicinal resources, cost-effective, and exhibit considerable adaptability and efficacy in the treatment of viral pneumonia, and have therefore emerged as the focus of antiviral research. In the treatment of influenza, TCM does not focus solely on the direct inhibition of viral replication but instead emphasizes a holistic approach based on the principles of syndrome differentiation and personalized therapy. This multi-targeted approach aims to alleviate the clinical symptoms of influenza infections and modulate host immunity, thereby mitigating the progression of inflammation and exerting comprehensive anti-influenza effects.[8]

Artemisia annua and Scutellaria baicalensis Georgi (skullcap) have been utilized in various TCM prescriptions since ancient times for the prevention and treatment of influenza. Previous studies have demonstrated that artesunate, extracted from *Artemisia annua*, can inhibit the activity of phosphodiesterase 4 (PDE4), suppress extracellular signal-regulated kinase/mitogen-activated protein kinase (ERK/MAPK) signaling pathways, and inhibit the nuclear export of viral ribonucleoprotein (vRNP) complexes of IAV.[9] It has been demonstrated that artesunate also exerts therapeutic effects on IAV-induced pneumonia by inhibiting the activation of the Toll-like receptor 4/RELA (TLR4/p65) signaling pathway and exerting anti-inflammatory effects.[10] Leaf extracts of *Artemisia annua* have been shown to inhibit influenza virus infections by targeting vRNPs and suppressing mitochondria-mediated apoptosis.[11] It has been demonstrated that nanovesicles derived from *Artemisia annua* modulate alveolar macrophages and mitochondrial adaptation, thereby alleviating acute lung injury (ALI) and viral pneumonia.[12] *Scutellaria baicalensis Georgi (skullcap)* also exhibits significant antiviral,[13–15] anti-inflammatory,[16,17] and immunomodulatory[18,19] effects, which are mediated via the activation of nuclear factor erythroid 2-related factor 2 (Nrf2) in response to H1N1 influenza virus infections.[20] Given the unique advantages of TCM in the treatment of influenza, recent years have witnessed an increase in the number of innovative approaches to the modernization of TCM. For instance, nanotechnology has been widely applied in the research and development of novel TCM-based therapeutics with various biological activities, including TCM-derived exosomes[21,22] and TCM-based carbon dots (CDs).[23,24] As natural nano-preparations, these systems possess unique properties, including favorable water solubility, biocompatibility, low cost of synthesis, and low toxicity, and they exhibit significant regulatory effects in wound repair, modulation of anti-inflammatory immune responses, and drug delivery. As a class of nanomaterials with unique advantages and broad application potential, TCM-based CDs have gained significant interest in the field of carbon nanomaterials due to their characteristic ultra-small size (< 10 nm), and have been extensively investigated both in China and internationally. They have been widely applied in drug delivery, bioimaging studies, and the treatment of various diseases.[23,25] At present, CDs are being investigated for the development of effective drug delivery systems, and studies have demonstrated that this novel nanocarrier can significantly enhance drug targeting and bioavailability, while substantially improving therapeutic efficacy.[26,27] As a promising nanotherapeutic approach, TCM-based CDs offer significant advantages in antiviral therapy. For instance, licorice-derived glycyrrhizic acid CDs have been found to exhibit enhance antiviral activity against IAVs, and their therapeutic efficacy is nearly three-fold that of free glycyrrhizic acid.[28] Their antiviral effects are likely mediated via the inhibition of IAV internalization, viral genome replication, neuraminidase activity, and infection-induced inflammation. These studies provide novel insights for the development of TCM-based CDs and their potential application in the therapeutic management of influenza. This study utilizes the unique nanoscale characteristics of CDs and proposes the following core hypothesis: 1) the nanoscale dimensions and surface characteristics of this system enhance cellular uptake efficiency; and 2) the synthesized multifunctional CDs-based carrier system enables efficient drug loading and targeted delivery of therapeutic agents. 3) Based on the anti-inflammatory properties of QH-CDs nanomaterials and traditional Chinese medicine precursors, we hypothesize that they specifically inhibit the activation of the NLRP3 inflammasome, thereby exerting a therapeutic effect against H1N1 influenza pneumonia.

To test this hypothesis, we designed a series of experiments: first, using in vivo experiments to verify their efficacy in improving pneumonia phenotypes; then, by detecting the expression and activation levels of key pathway proteins and mRNA, to confirm their inhibitory effect on the NLRP3 pathway. All experiments are carried out to validate this hypothesis.

Methods and Materials

Experimental Animals and Viral Strain

Fifty-six male ICR mice, weighing 18 ± 2 g, were purchased from Hangzhou Medical College. All the animal experiments were conducted in accordance with the institutional guidelines and approved by the relevant ethics committee (Institute of Basic Medicine and Oncology, Chinese Academy of Sciences Animal Experiments Ethical Inspection of Zhejiang Center of Laboratory Animals 2024R0120301). All the procedures involving animals were conducted in accordance with the ethical policies and procedures approved by the Zhejiang Laboratory Animal Center of Hangzhou Medical College (Quality Certification No. SCXK (Zhe) 2021–0002) and Experimental Facilities Certification No. SYXK (Zhe) 2024–0009).

The IAV strain A/PR/8/34 (H1N1) was kindly donated by the Institute of Basic Medical Sciences and Oncology, Chinese Academy of Sciences, with a 50% tissue culture infectious dose ($TCID_{50}$) of $10^{-3.4}$. To preserve viral infectivity, the strain was stored under appropriate conditions at −80 °C. Prior to each experiment, appropriate sample aliquots were prepared as required to avoid repeated freeze-thaw cycles. The medicinal materials used in this study were purchased from the Traditional Chinese Medicine Outpatient Department of Zhejiang Chinese Medical University.

Synthesis and Characterization of CDs Co-Derived from Artemisia annua and Scutellaria baicalensis (QH-CDs)

Artemisia annua and *Scutellaria baicalensis* (skullcap) were powdered and thoroughly mixed in a defined ratio. Then 0.1 g of the medicinal powder was transferred to a polytetrafluoroethylene-lined reaction kettle, followed by the addition of 30 mL of ultrapure water. The mixture was subsequently reacted at 180 °C in an oven for 6 h. The reaction kettle was opened after the reaction mixture cooled to room temperature (25 °C), and the contents were centrifuged at 10000 x *g* for 1 h. The supernatant was collected and filtered with a 0.22 μm membrane filter to further remove any precipitate. The solution was transferred to a dialysis bag with a molecular weight cut-off of 500 Da and dialyzed with ultrapure water for 24 h, with the ultrapure water replaced every 6 h. The dialyzed solution was collected and freeze-dried under vacuum to obtain the purified drug-loaded CDs. The morphological and structural characteristics of the QH-CDs were analyzed by transmission electron microscopy (TEM; H-7650, Hitachi, Ltd., Japan) operated at an accelerating voltage of 120 kV, with an operating power supply of 220 V (±10%) and 50 Hz, an operating temperature of 15–20 °C, and operating humidity below 80%. The particle size distribution of the QH-CDs was statistically evaluated from the TEM images using Image J software. The absorption peaks of the QH-CDs were characterized by ultraviolet-visible (UV-Vis) absorption spectroscopy, while their X-ray diffraction (XRD) patterns were determined with an X-ray diffractometer (XRD-7000, Shimadzu, Japan) at a scanning range of 5–90° and a scanning rate of 5°/min.

QH-CDs in vivo Safety Evaluation

Healthy SPF-grade ICR male mice, weighing 15–18 g, were acclimated and then randomly assigned to two groups (n = 5 per group): a control group that received normal saline and a treatment group that was administered QH-CDs.

The mice were provided *ad libitum* access to standard feed and drinking water, and were maintained at a room temperature of 25 ± 2 °C with a relative humidity of 50–60%, under a 12 h/12 h light/dark cycle. All the animal experiments were conducted in strict accordance with the regulations and general guidelines for the care and use of laboratory animals. After 14 days of intragastric administration, the mice were anesthetized with isoflurane and subsequently euthanized by cervical dislocation. The collected blood samples were centrifuged at 3000 x *g* for 15 min, and the supernatant was collected for further analyses. The serum levels of alanine aminotransferase (ALT), aspartate aminotransferase (AST), blood urea nitrogen (BUN), and creatinine (CREA) were measured. The heart, liver, spleen, lung, kidney, and colon tissues were fixed in 4% paraformaldehyde solution, embedded in paraffin, and sectioned into 4 μm-thick slices. The tissue sections were then stained with hematoxylin and eosin (H&E), followed by microscopic examination and image acquisition (C13210-01, Hamamatsu, Japan).

The in-vivo Studies Using Animal Model

Healthy SPF-grade ICR male mice, weighing 15–18 g, were acclimated and randomly divided into seven groups (n = 8 per group): a control group that received normal saline; a model group infected with H1N1; a positive group treated with oseltamivir; a low-dose QH-CD group (30 mg/kg); a medium dose QH-CD group (60 mg/kg); and a high-dose group (90 mg/kg) that received a herbal decoction of *Artemisia annua* and *Scutellaria baicalensis*. Then, 10 g each of *Artemisia annua* and *Scutellaria baicalensis* were soaked in purified water for 30 min. Extraction was performed by decoction with purified water at a solvent-to-material ratio of 8:1 (w/w) and boiled for 1 h. The extraction procedure was repeated twice. The volume was adjusted to 77 mL using purified water, yielding a decoction with a final concentration of 33 mg/mL.

The mice were provided *ad libitum* access to standard feed and drinking water, and were maintained at a room temperature of 25 ± 2 °C with a relative humidity of 50–60%, under a 12 h/12 h light/dark cycle. All the animal experiments were conducted in strict accordance with the regulations and general guidelines on the care and use of laboratory animals. The IAV infection model was established on the fourth day by nasal instillation of 50 μL of a suspension of H1N1 virus following anesthesia with isoflurane gas. The mice in the control group received an equal volume of normal saline. The changes in body weight were recorded and monitored on a daily basis following infection to assess disease progression and the effects of the respective interventions. The mice received continuous administration until the fifth day, following which they were anesthetized with isoflurane and euthanized by cervical dislocation. The mice were humanely sacrificed and blood samples were collected from the retro-orbital sinuses, centrifuged at 3000 xg for 15 min, and the supernatant was collected for further analyses. The serum levels of interleukin (IL)-6, IL-17A, interferon (IFN)-β, tumor necrosis factor (TNF)-α, and other cytokines were measured by enzyme-linked immunosorbent assay (ELISA), in strict accordance with the requirements of the ELISA kits. The lung tissues were fixed in 4% paraformaldehyde solution, embedded in paraffin, and sectioned into 4 μm-thick slices. The histopathological sections were prepared after H&E staining, followed by microscopic examination and image acquisition.

Systemic Inflammatory Assessment

The mice were sacrificed on the fifth day following infection, and the lung tissues were excised and weighed for calculating the lung index. The lung and spleen indices were calculated using the following formulae:

Lung index = (weight of lung/body weight) × 100%

Spleen index = (weight of spleen/body weight) × 100%

The lung tissues were fixed in 4% paraformaldehyde, embedded in paraffin, sectioned, and stained with H&E, following which the histopathological changes were examined under a microscope (C13210-01, Hamamatsu, Japan). The levels of TNF-α, IL-1β, IL-6, and IL-18 in the supernatant were measured using commercially available ELISA kits purchased from ABclonal (MA, USA). All the experiments were performed in accordance with the manufacturer's instructions.

Transcriptomic Analysis

Total RNA was extracted from the samples and purified using TRIzol reagent (Cat. No. 15596018; Thermo Fisher Scientific, CA, USA) according to the manufacturer's protocol. The quantity and purity of the total RNA were subsequently evaluated using a NanoDrop ND-1000 spectrophotometer (NanoDrop, Wilmington, DE, USA), and the integrity of the RNA was assessed using a Bioanalyzer 2100 system (Agilent, CA, USA). Samples with a concentration > 50 ng/μL, RNA integrity number (RIN) > 7.0, and total RNA yield > 1 μg were considered suitable for subsequent experimentation. The mRNA was specifically captured through its polyadenylated (polyA) tails using oligo(dT) magnetic beads (Dynabeads Oligo(dT); Cat. No. 25–61005; Thermo Fisher Scientific, CA, USA) and purified through two rounds of enrichment. The captured mRNA was subjected to high-temperature fragmentation using the NEBNext® Magnesium RNA Fragmentation Module (NEB, Cat. No. E6150S, USA) at 94 °C for 5–7 min. The fragmented RNA was used for cDNA synthesis using SuperScriptTM II Reverse Transcriptase (Cat. No. 1896649; Invitrogen, CA, USA). The resulting DNA-RNA duplex was converted into a DNA duplex using *Escherichia coli* DNA polymerase I (Cat. No. m0209; NEB,

USA), RNase H (Cat. No. m0297; NEB, USA), and dUTP solution (Cat. No. R0133; Thermo Fisher Scientific, CA, USA). The ends of the double-stranded DNA were end-repaired to generate blunt ends, followed by the addition of an adenine (A) to the 3′ ends to enable ligation with adapters containing a thymine (T) overhang. The DNA fragments were subsequently screened based on size and purified using magnetic beads. The second strand was digested using Uracil-DNA Glycosylase (Cat. No. m0280; NEB, MA, USA) and pre-denatured at 95 °C for 3 min, followed by denaturation at 98 °C for 8 cycles of 15 sec each, annealing at 60 °C for 15 sec, extension at 72 °C for 30 sec, and a final extension at 72 °C for 5 min. This procedure generated a strand-specific library with an average fragment size of 300 ± 50 bp. Paired-end sequencing was finally performed on an Illumina Novaseq^{TM} 6000 system (LC-Bio Technology Co., Ltd., Hangzhou, China), according to the standard operational procedure, using the PE150 sequencing mode.

Gene Expression Analysis of Key Factors by RT-qPCR

The tissues were initially lysed using TRIzol reagent to extract the total RNA. Then 1 μg of the total RNA was reverse transcribed into cDNA using a reverse transcription kit. The resulting cDNA was amplified by real-time PCR, and the expression levels of the target genes were calculated using the $2^{-\Delta\Delta Ct}$ method, with *β-actin* as the internal reference gene for normalization. All the technical replicates were performed in at least triplicate to ensure data reliability.

Detection of Protein Expression Levels by Western Blotting

Total cellular protein was extracted using a total protein extraction kit containing a protease inhibitor cocktail, and quantified using the bicinchoninic acid (BCA) assay. The proteins were separated by sodium dodecyl sulfate-polyacrylamide gel electrophoresis (SDS-PAGE) using an 8–12% gradient resolving gel and a 5% stacking gel. Then 60 μg of total protein (volume 10–15 μL) was loaded per well, and electrophoresis was performed for approximately 2 h at 60 V for the stacking gel and at 80 V for the resolving gel. Following electrophoresis, the polyvinylidene fluoride (PVDF) membrane was activated by incubating in methanol for 20 seconds. The membrane was then equilibrated with the gel in Tris-Glycine transfer buffer containing 5% methanol, and the protein bands were transferred at a constant voltage of 100 V for 2 h at 4 °C. Following transfer, the membrane was blocked with Tris-buffered saline with Tween (TBST) containing 5% bovine serum albumin (BSA) for 1 h at room temperature (25 °C). The membrane was then rinsed thrice with TBST for 5 min each, incubated overnight at 4 °C with the primary antibody diluted in TBST containing 3% BSA, and finally rinsed 4 times with TBST for 5 min each. The membrane was subsequently incubated at room temperature (20–25 °C) for 1 h with the secondary antibody dissolved in TBST containing 3% BSA at a specified proportion, and subsequently washed five times with TBST for 5 min each. An ECL working solution was subsequently prepared using SuperSignal® West Dura Extended Duration Substrate, according to the manufacturer's instructions. The membrane was then incubated with approximately 1 mL of the ECL solution for 1 min at room temperature, following which excess ECL reagent was removed. The membrane was then sealed with plastic wrap, placed in an exposure cassette with an X-ray film, and exposed for 5–10 min, followed by development and fixation to complete the Western blotting procedure.

Statistical Analyses

All the statistical analyses were performed using GraphPad Prism (v9.0). One-way analysis of variance (ANOVA) was used for between-group comparisons, followed by with Tukey's post-hoc test, or unpaired t-tests. A p-value < 0.05 was considered to be statistically significant.

Results

Morphological Characterization of QH-CDs

TEM revealed that the QH-CDs were spherical in shape, uniformly distributed, and had an average particle size of less than 10 nm (Figure 1A). The XRD pattern of the QH-CDs exhibited a characteristic broad peak around 22° (Figure 1B), which was consistent with the plane commonly observed in CDs, as reported in previous studies.[29] The UV-Vis spectrum of the QH-CDs showed a small peak at 220–230 nm (Figure 1C). The shoulder observed around 225 nm is likely

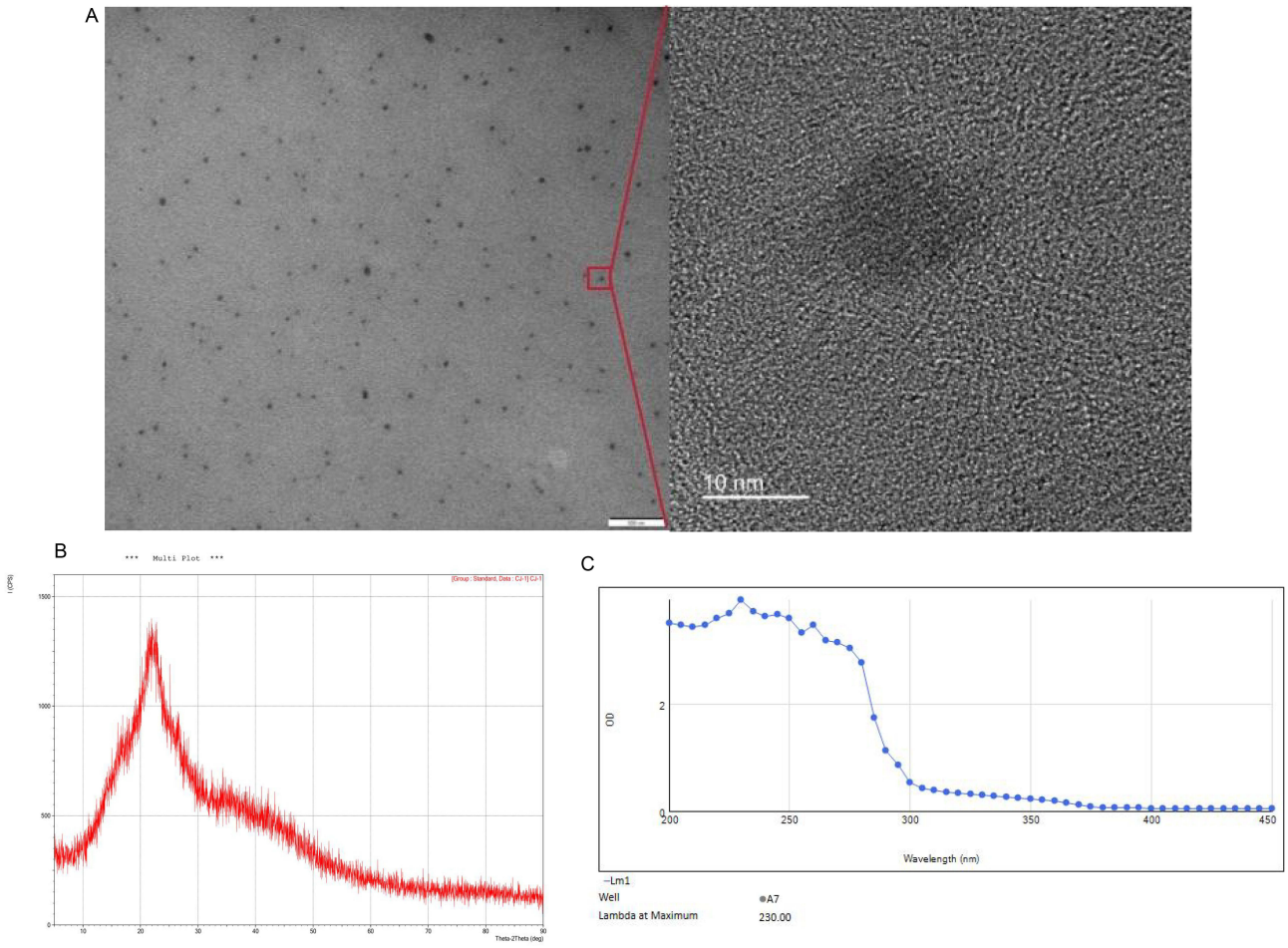

Figure 1 Morphological characterization of synthesized QH-CDs. (**A**) Representative TEM images, (**B**) XRD pattern, and (**C**) UV-Vis spectrum of the synthesized QH-CDs.

attributable to the n-π* transition of surface carbonyl or carboxyl (C=O) groups, thus providing additional support for the structural characterization of the QH-CDs.

Assessment of in vivo Safety of QH-CDs

All the mice survived throughout the experiment, even at the highest administered dose and across all dosing frequencies. The liver and kidney function indicators (ALT, AST, BUN, and CREA) of mice were tested. The results demonstrated that all the indices remained within the normal reference range for healthy mice, and no abnormal changes were observed in the liver and kidney function indices, indicating that the treatments did not induce any apparent hepatotoxicity or nephrotoxicity in mice. Statistical analysis revealed no significant differences in the levels of ALT (Figure 2A), AST (Figure 2B), BUN (Figure 2C), and CREA (Figure 2D) between the control and different treatment groups ($p > 0.05$).

Histological examination revealed that the structural integrity of the cardiac tissues was preserved, with neatly arranged myocardial fibers, patent coronary arteries, and no evidence of hypertrophy, fibrosis, or inflammatory lesions. The liver tissues exhibited a normal histological structure, with no pathological changes such as inflammation, necrosis, or fibrosis. The white and red pulp of the spleen exhibited well-defined structures, with well-filled blood sinuses, and no evidence of abnormal hyperplasia or infarction. The alveolar structure of the lung tissues was intact, the bronchial epithelium was arranged in an orderly manner, and no inflammatory infiltration was observed in the interstitium. The renal cortex and medulla were clearly demarcated, with normal glomerular and tubular structures, and regularly arranged blood vessels. The intestinal wall exhibited a complete four-layer structure, the intestinal glands were arranged in an

https://doi.org/10.2147/IJN.S566658

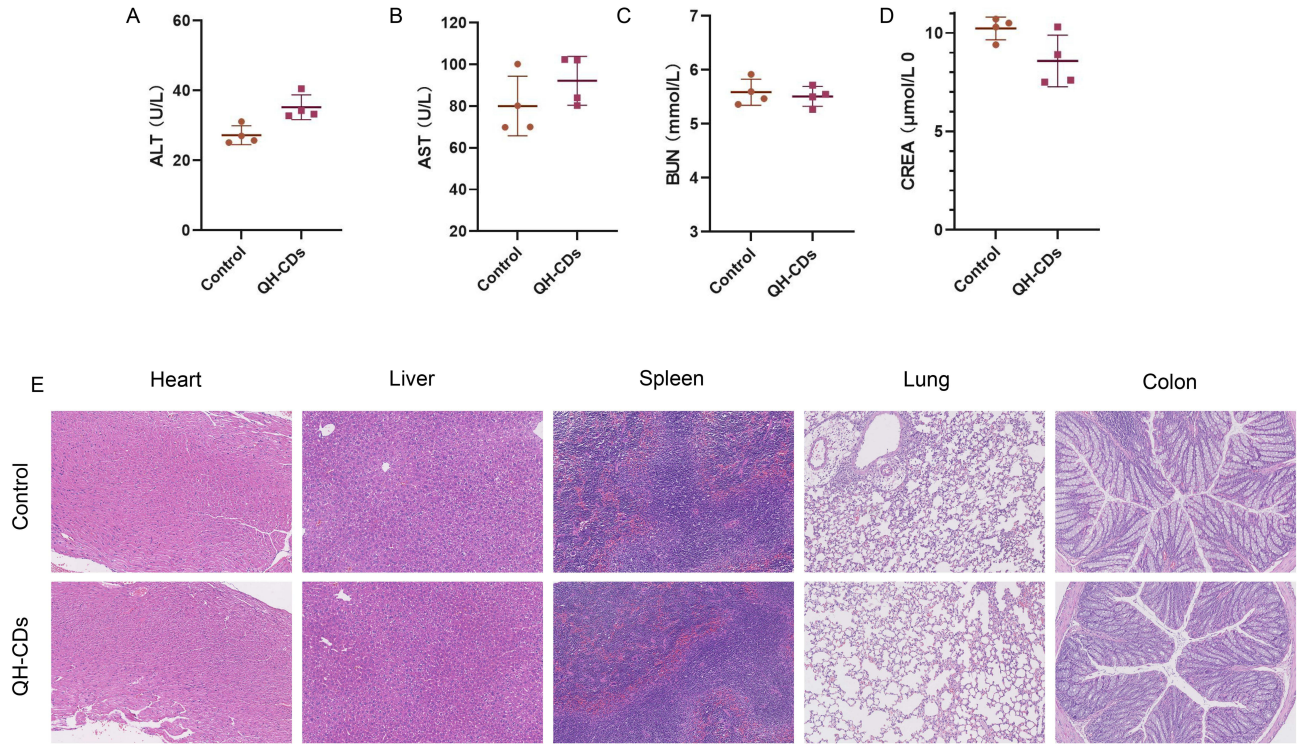

Figure 2 Assessment of in vivo safety profile of QH-CDs. (**A**–**D**) Serum levels of ALT, AST, BUN, and CREA in the control and different treatment groups. (**E**) Representative H&E-stained histological images of the heart, liver, spleen, kidney, lung, and colon tissues from the control and different treatment groups (scale bar: 200 μm).

orderly manner, and the lymphoid nodules in the lamina propria displayed a normal distribution. Pathological changes, such as inflammatory cell infiltration, edema, hemorrhage, necrosis, or fibrosis, were not observed in any organ. All the histological features appeared normal, indicating that the structural and functional characteristics of all the organs remained preserved under the given experimental conditions (Figure 2E).

These results collectively indicate that the QH-CDs possess good biocompatibility and low in vivo toxicity.

Evaluation of General Health Status of Mice Using Lung and Spleen Indices and in vivo Inflammatory Factor Levels

The model group exhibited higher mortality (Figure 3A), more significant weight loss (Figure 3B), an elevated lung index (Figure 3C), and a reduced spleen index (Figure 3C) on the fifth day after influenza virus infection, compared to those observed in the control group. However, treatment with QH-CDs mitigated weight loss (Figure 3B), elevated the spleen index (Figure 3C), and lowered the lung index (Figure 3C). Additionally, the serum levels of various inflammatory factors (Figure 3D), including transforming growth factor-β1 (TGF-β1), IL-6, and TNF-α, decreased significantly following the administration of QH-CDs, indicating that the treatment partially alleviated pulmonary symptoms and reduced inflammation following IAV infection.

Histopathological Examination of Lung Tissues

H&E staining of the lung tissues revealed that the pulmonary histology of the control group remained normal (Figure 4A and B), with intact alveolar septa and normal alveolar size. In contrast, the model group exhibited substantial lymphocytic infiltration around the pulmonary small blood vessels and bronchioles, accompanied by the widening of alveolar septa.

Both oseltamivir and QH-CDs significantly alleviated pulmonary inflammation, as evidenced by reduced inflammatory cell infiltration, decreased vasodilation, and overall improvement in lung pathology. Histological examination revealed that the lung tissues of IAV-infected mice exhibited marked edema and congestion, which were significantly alleviated following treatment with oseltamivir and QH-CDs. The pathological damage to the lung tissues of IAV-

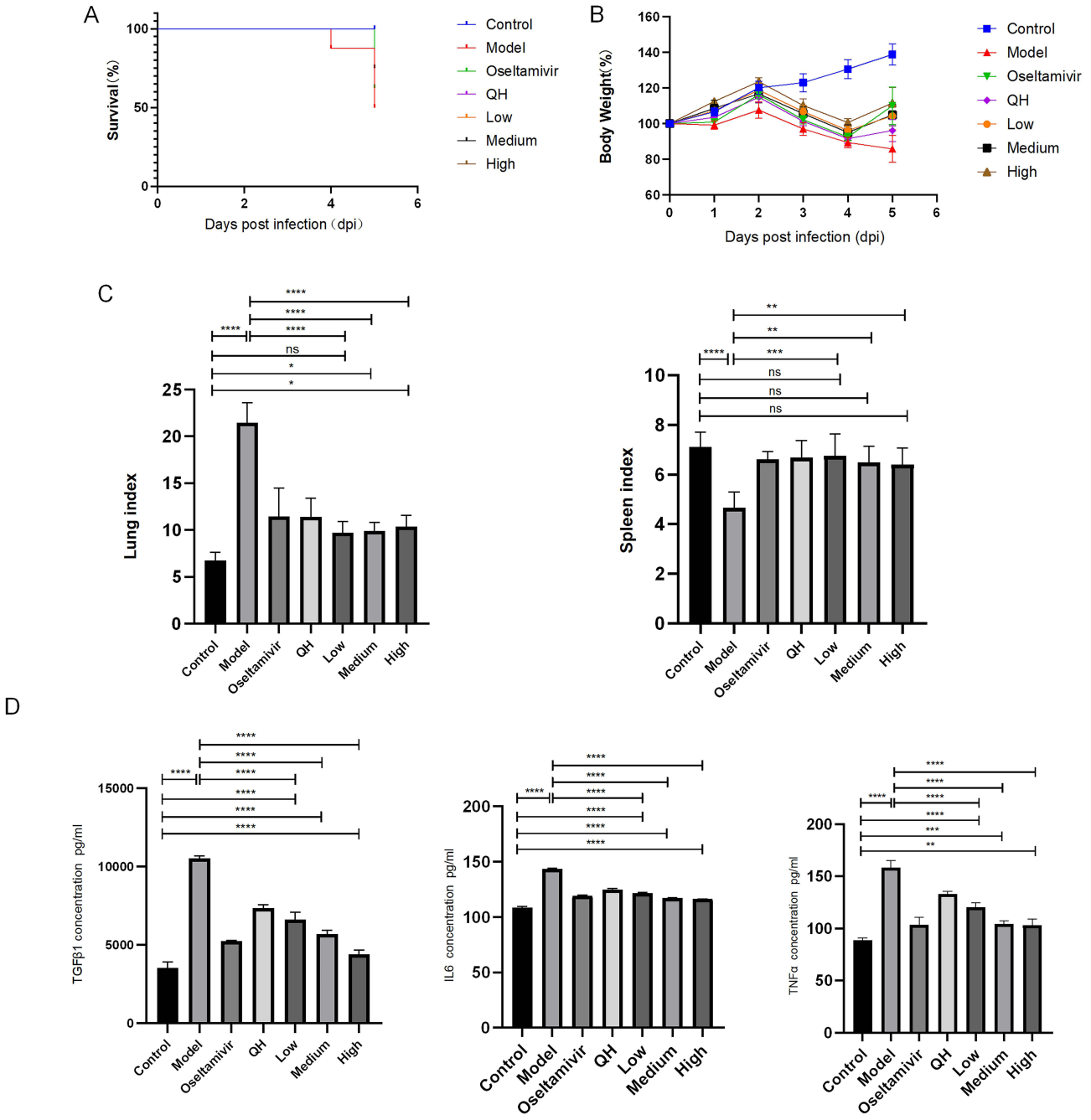

Figure 3 Effect of QH-CD on the general health status of IAV-infected mice. (**A**) Survival rate of mice post-infection. (**B**) Changes in the body weights of the different treatment groups, compared to that of the control group, on different days post-infection. Comparative analysis of the (**C**) lung and spleen indices and (**D**) the serum levels of the inflammatory factors, TGF-β1, IL-6, and TNF-α, across the control and treatment groups; ns: not Significant, *p< 0.1, **p < 0.01, ***p < 0.001, and ****p < 0.0001.

infected mice was significantly alleviated following treatment with QH-CDs. These findings collectively indicate that the QH-CDs effectively alleviated the pulmonary damage induced by IAV infection.

Transcriptomic Analyses

The differentially expressed genes between the control and different treatment groups were identified using the following screening criteria: $|\log_2(\text{fold change (FC)})| \geq 1$ and $p < 0.05$, and the results are presented in Figure 5. The results of correlation analysis of gene expression levels across samples are presented in Figure 5A, and the number of differentially expressed genes in each comparison group is shown in Figure 5B. Compared to that in the control group, 1463 and 1056

https://doi.org/10.2147/IJN.S566658

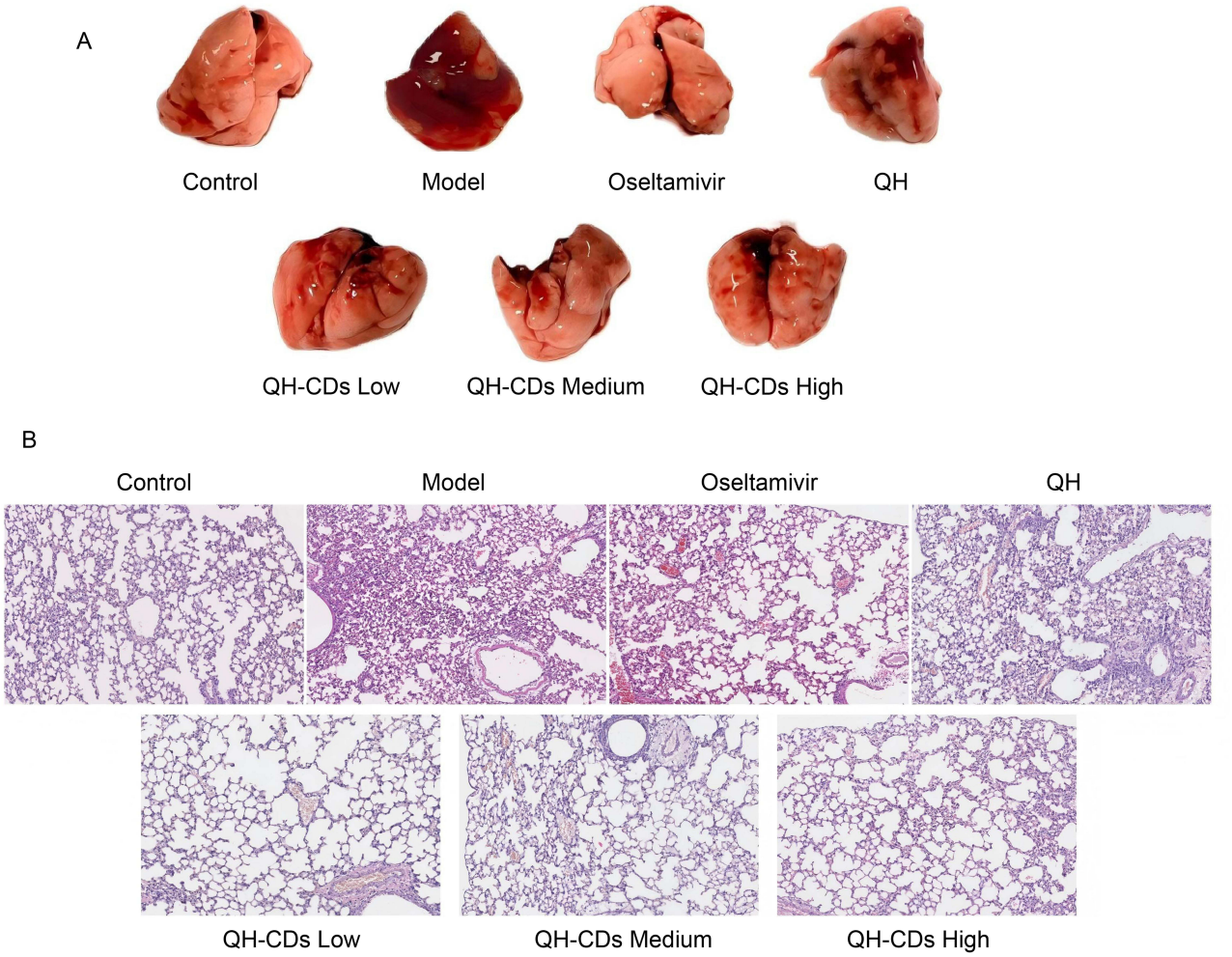

Figure 4 Effects of QH-CD administration on lung histology in IAV-infected mice. (**A**) Representative macroscopic image of the whole lungs. (**B**) Representative H&E-stained sections of lung tissues obtained by scanning (scale bar: 200 μm).

genes were identified as upregulated and downregulated, respectively, in the high-dose QH-CD group, while 1115 upregulated and 406 downregulated genes were identified in the low-dose QH-CD group. A total of 1509 and 390 genes were found to be upregulated and downregulated, respectively, in the medium-dose QH-CD group, while 2575 upregulated and 3038 downregulated genes were identified in the model group. Compared to that in the model group, 12 and 206 genes were identified as upregulated and downregulated, respectively, in the high-dose QH-CD group, while 12 upregulated and 235 downregulated genes were identified in the low-dose QH-CD group (Figure 5C and D). Additionally, 16 and 153 genes were found to be upregulated and downregulated, respectively, in the medium-dose QH-CD group. Gene ontology (GO) (Figure 5E) and Kyoto Encyclopedia of Genes and Genomes (KEGG) (Figure 5F) pathway enrichment analyses revealed that the differentially expressed genes were primarily involved in immune regulation, cytokine activity, and inflammatory signaling pathways, particularly the NOD-, LRR-, and pyrin domain-containing protein 3 (NLRP3) inflammasome signaling pathway.

Effect of QH-CDs Administration on Pulmonary Viral Load and NLRP3 Inflammasome Pathway mRNA Expression in Mice with IAV-Induced Pneumonia

To investigate the effects of treatment with QH-CDs on the NLRP3 inflammasome signaling pathway in the lung tissues of mice with IAV-induced pneumonia, the mRNA expression levels of TLR4, NLRP3, caspase-1, IL-1β, IL-6, IFN-β1, and IL-17A in the lung tissues were detected by RT-qPCR. As depicted in Figure 6, the mRNA expression levels of

TLR4 (Figure 6A), NLRP3 (Figure 6B), caspase-1 (Figure 6C), and IL-1β (Figure 6D), IL-6 (Figure 6F), IFN-β1 (Figure 6G), and IL-17A (Figure 6H) were significantly upregulated in the model group ($p < 0.05$), compared to those in the control group, while treatment with QH-CDs significantly downregulated the mRNA expression of these genes. The gene encoding the IAV nucleoprotein (NP) plays a critical role in viral replication. RT-qPCR analysis revealed that the mRNA expression levels of the *NP* gene (Figure 6E) were not significantly downregulated in the groups treated with oseltamivir or QH-CDs ($p < 0.05$). Analysis of viral titers in the lung tissues revealed that both QH-CDs and oseltamivir reduced the viral load, with a statistically significant difference observed between the oseltamivir-treated and model groups ($p < 0.05$). RT-qPCR analysis revealed that treatment with QH-CDs significantly downregulated the expression of host inflammation-related genes.

Effect of QH-CDs on Viral Load and the NLRP3 Inflammasome Pathway in the Lung Tissues of Mice with IAV-Induced Pneumonia

The effect of treatment with QH-CDs on the NLRP3 inflammasome signaling pathway in the lung tissues of IAV-infected mice was investigated by measuring the expression levels of p-NF-κB p65, NLRP3, cleaved caspase-1, and cleaved IL-1β proteins by Western blotting. The expression levels of components of the NLRP3 inflammasome signaling pathway in the lung tissues were additionally assessed by Western blotting (Figure 7A). The expression levels of p-NF-κB p65, NLRP3, caspase-1, and IL-1β were found to be significantly upregulated in the model group compared to those in the control ($p < 0.05$), while treatment with QH-CDs significantly downregulated their expression levels. These findings are consistent with the previously observed changes in mRNA expression levels. The effects of QH-CDs are likely mediated

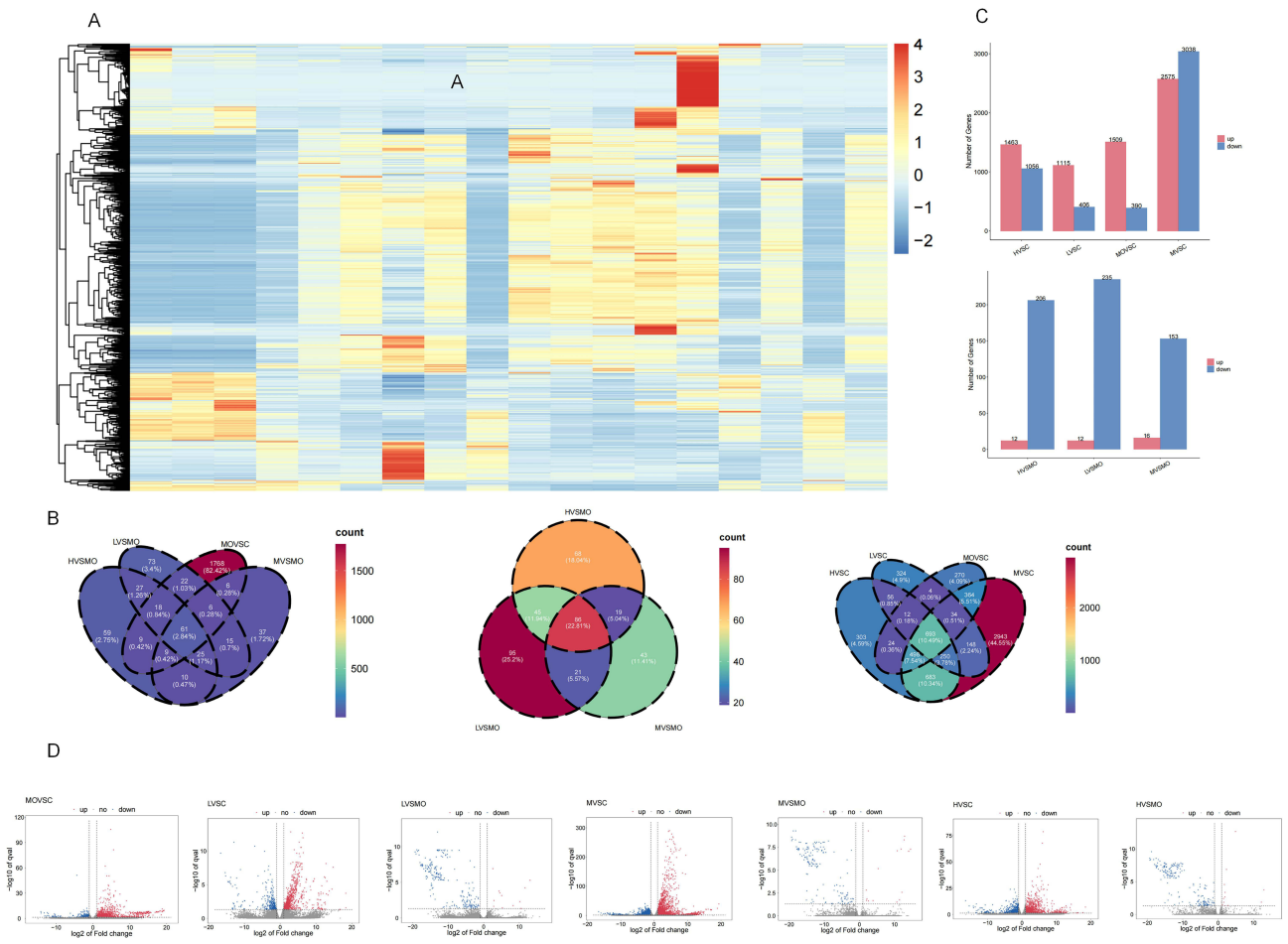

Figure 5 continued.

https://doi.org/10.2147/IJN.S566658

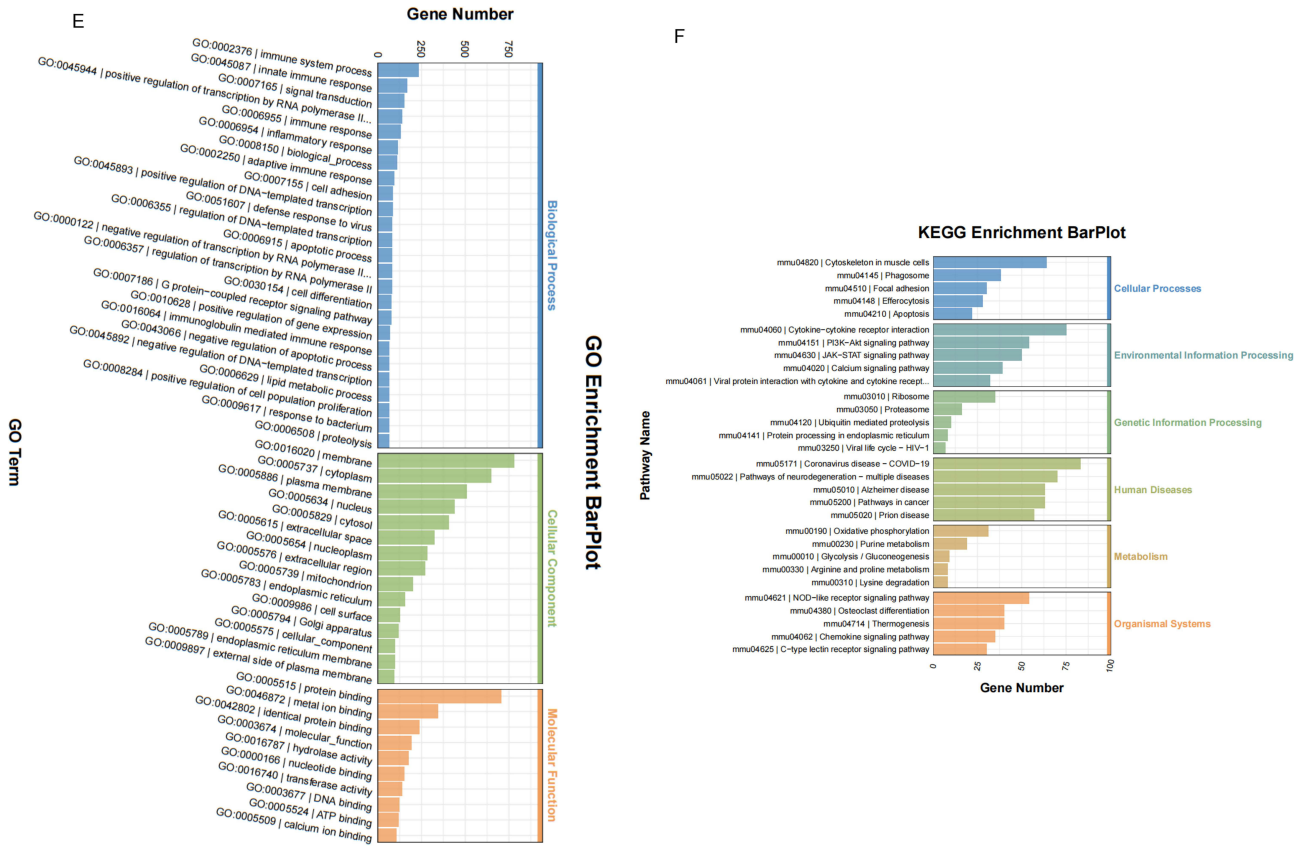

Figure 5 Transcriptomic analysis of lung tissues. (**A**) Correlation analysis of gene expression levels across samples. (**B**) Number of differentially expressed genes in each comparison group, including upregulated ($log_2FC \geq 1$ and $q < 0.05$) and downregulated ($log_2FC \leq -1$ and $q < 0.05$) genes. (**C**) Venn diagrams depicting the overlap of differentially expressed genes in the different control and treatment groups. (**D**) Volcano plots depicting differential gene expression. The red and blue dots denote the differentially expressed genes that were significantly upregulated and downregulated, respectively, while the gray dots represent genes without significant differential expression. Results of (**E**) GO and (**F**) KEGG enrichment analyses. (C: control group; Mo: model group; L: low QH-CD group; M: medium QH-CD group; H: high QH-CD group).

via the inhibition of viral RNA-induced phosphorylation of p-NF-κB p65, suppression of inflammasome assembly, or interference with the release of mature IL-1β. These results suggest that QH-CDs may effectively mitigate inflammatory damage in viral pneumonia by selectively downregulating the expression of key proteins, including p-NF-κB p65 (Figure 7B), NLRP3 (Figure 7C), cleaved caspase-1 (Figure 7D), and cleaved IL-1β (Figure 7E). TCM has a long-standing history and offers distinct therapeutic advantages in the prevention and treatment of influenza and other externally contracted febrile illnesses. Numerous studies have demonstrated that TCM compounds exert antiviral and immunomodulatory effects by acting on multiple targets and signaling pathways.[30,31] Contemporary studies have demonstrated that *Artemisia annua* and *Scutellaria baicalensis* exhibit significant anti-inflammatory[16,32,33] and antiviral[34–36] activities. These effects are particularly notable in the context of the *Artemisia annua-Scutellaria baicalensis* decoction, which is derived from the classic TCM prescription, *Artemisia annua-Scutellaria* clear gall decoction. In recent years, studies on the nanochemistry of TCM drugs have provided novel insights into the contemporary pharmacological mechanisms underlying traditional formulations.[12] As a novel type of nanomaterial, TCM-based CDs offer distinct advantages in terms of anti-inflammatory and antiviral properties. TCM-derived CDs not only retain the multi-component synergistic therapeutic properties of TCM formulations, but also possess the unique surface properties and nanoscale characteristics of nanomaterials, enabling them to exert potent anti-inflammatory and antiviral effects via multiple signaling pathways. In this study, CDs were synthesized for the first time using *Artemisia annua* and *Scutellaria baicalensis* as precursors, yielding particles with an average diameter of approximately 10 nm. The present study builds on recent findings that the nano-processing of TCM herbs enhances biofilm penetration and target specificity.[37–39] The

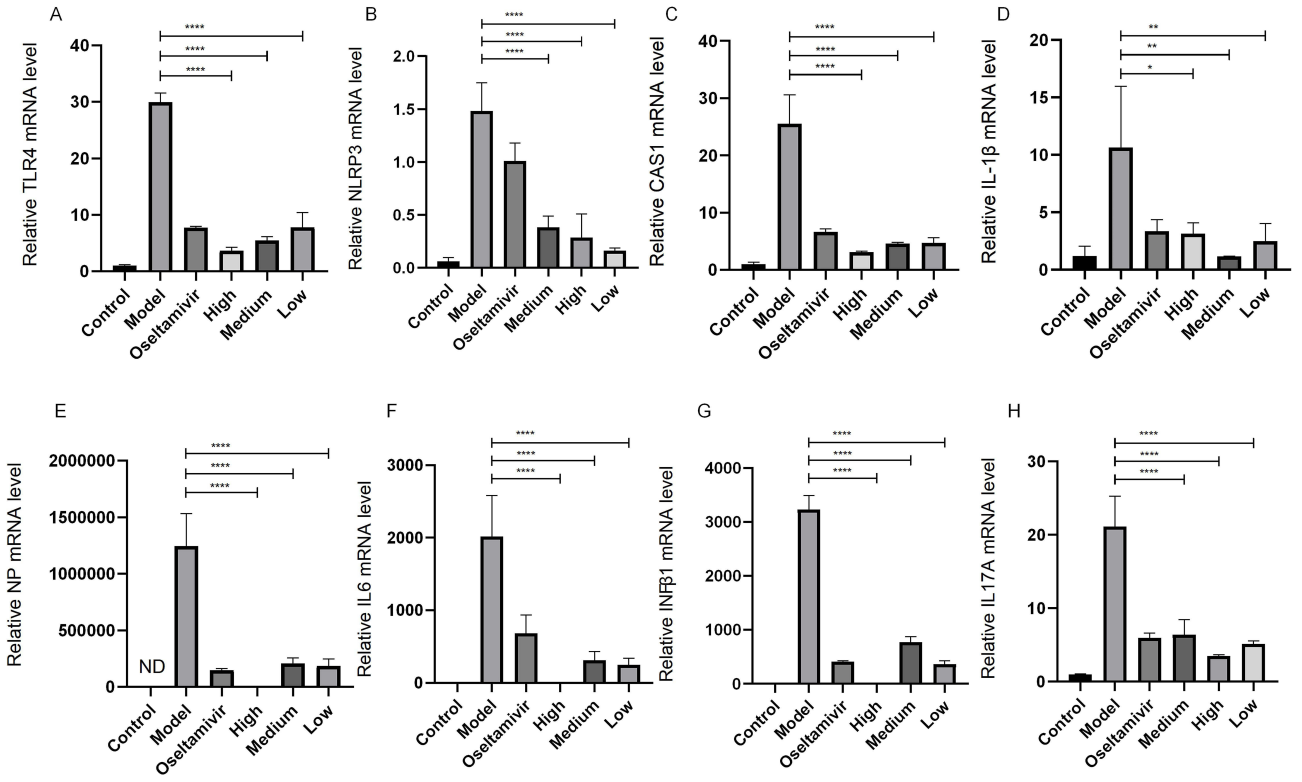

Figure 6 mRNA expression levels of genes in the NLRP3 inflammasome pathway in the lung tissues of mice treated with QH-CDs. Relative mRNA expression levels of (**A**) TLR4, (**B**) NLRP3, (**C**) caspase-1, (**D**) IL-1β, (**E**) NP, (**F**) IL-6, (**G**) IFN-β1, and (**H**) IL-17A in the lung tissues of the control and different treatment groups; ns: not Significant, *$p < 0.05$, **$p < 0.01$, and ****$p < 0.0001$.

findings provide a robust scientific basis for the development of novel anti-influenza drugs, especially for the treatment of IAV infections and the associated inflammatory responses.

Recent studies have increasingly emphasized that the aberrant activation of the NLRP3 inflammasome signaling axis plays a critical role in various inflammatory diseases. It has been demonstrated that the activation of the NLRP3 inflammasome pathway induces the pyroptosis of alveolar epithelial cells, increases vascular permeability, promotes the activation of macrophages, and enhances neutrophil dysfunction, thereby playing a critical role in the pathogenesis of ALI.[40] The overactivation of the NLRP3 inflammasome represents a central mechanism underlying lung injury in viral pneumonia.

Discussion

In this study, we successfully synthesized water-soluble, uniformly dispersed fluorescent *Artemisia annua-Scutellaria baicalensis* herb pair CDs (QH-CDs) with an average particle size of approximately 10 nm, using artemisinin and baicalin (QH) as precursor compounds. The characterization data revealed that the material exhibited a typical CD structure and favorable biocompatibility. The administration of QH-CDs downregulated the p-NF-κB p65/NF-κB signaling pathway, suppressed caspase-1 cleavage, and reduced the maturation of IL-1β by inhibiting the activation of the NLRP3 inflammasome. In terms of immune regulation, the QH-CDs also downregulated the levels of pro-inflammatory cytokines, including TGF-β1, IL-6, and TNF-α. The results demonstrated that IAV infection significantly activated the NLRP3 inflammasome signaling pathway in the lung tissues of mice. This finding is consistent with previous research showing that berberine significantly mitigates pneumonia caused by influenza virus infection by targeting and inhibiting the activation of the NLRP3 inflammasome pathway.[41] The consistency of the findings further supports the scientific validity of the NLRP3 inflammasome as a key therapeutic target for the treatment of viral pneumonia. The principal findings demonstrate that QH-CDs exert significant protective effects against H1N1-induced lung injury, with evidence of potential dose-dependent efficacy. The therapeutic mechanism extends beyond a general

https://doi.org/10.2147/IJN.S566658

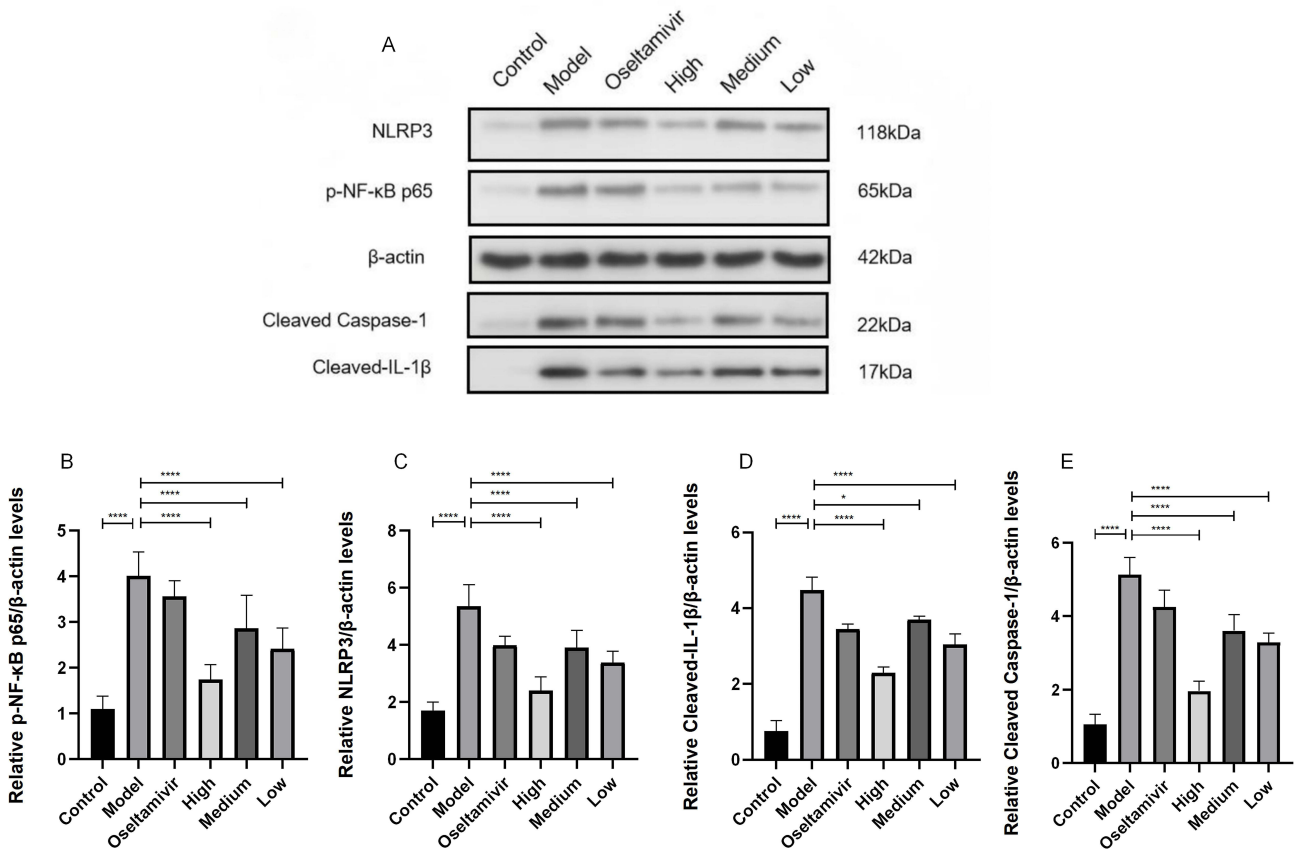

Figure 7 Changes in the pulmonary expression levels of proteins in the NLRP3 inflammasome pathway following treatment with QH-CDs. (**A**) Representative Western blots depicting the expression levels of proteins in the NLRP3 inflammasome pathway in the lung tissues of the control and treatment groups. Relative expression levels of (**B**) p-NF-κB p65, (**C**) NLRP3, (**D**) cleaved caspase-1, and (**E**) cleaved IL-1β proteins in the lung tissues of mice in the control and treatment groups; *p < 0.05, ****p < 0.0001.

anti-inflammatory effect and specifically involves the inhibition of NLRP3 inflammasome activation via the down-regulation of NLRP3 and caspase-1 protein and gene expression, thereby suppressing the downstream production of mature IL-1β. This mechanism represents a novel approach in existing studies on anti-inflammatory CDs derived from TCM formulations. The present study revealed alterations at the protein level and confirmed the regulatory effects of QH-CDs at the transcriptional level via mRNA analysis, suggesting that they likely modulate upstream signaling events of NLRP3, including the inhibition of NF-κB activation, thereby reducing the initiation of inflammasome priming at its source. This mechanism of action is more upstream compared with the mere suppression of assembled inflammasome activity. Consistent with the majority of previous studies, the complex composition of TCM precursors endows QH-CDs with abundant surface functional groups and high biocompatibility. Unlike CDs derived from single-herb precursors, QH-CDs originate from a compound herbal system. We hypothesize that the presence of multiple active ingredient precursors may introduce a higher number of heteroatoms (O, N) during carbonization, resulting in a more disordered and defect-rich carbon layer structure. This generates a more complex surface chemical "fingerprint", encompassing specific functional group ratios or spatial distributions, which is typically associated with enhanced catalytic or biological activity. This study found that QH-CDs can simultaneously inhibit the phosphorylation of NF-κB (p65) and the activation of Caspase-1 (p20). This finding is highly significant. Our results suggest that QH-CDs provide a more upstream and fundamental intervention. It can be inferred that simultaneously regulating both the "initiation" and "activation" stages may be a better strategy for treating excessive inflammation caused by viral infections. Therefore, we tend to believe that the action of QH-CDs is not simply "inhibition", but a form of "immune modulation". It does not completely block the necessary antiviral immunity (such as the early production of IFN-β), but precisely "trims" the later uncontrolled

inflammatory pathways (such as the NLRP3/IL-1β axis). This selective immune-modulating property is derived from its complex traditional Chinese medicine precursors and distinguishes it from conventional immunosuppressants.

Conclusion

The significance of this study lies in providing a novel "nanoscale" strategy to modernize TCM formulations by transforming complex components into structurally defined and functionally clarified nanomaterials; elucidating a precise anti-inflammatory mechanism mediated by carbon nanodots, directly supporting their potential as targeted nanomedicines for the NLRP3 pathway; and expanding the application prospects of CDs in the treatment of respiratory diseases.

Our future research aims to utilize XPS and complementary techniques to precisely characterize the surface chemical structure and active sites of QH-CDs; investigate the cellular uptake pathways of QH-CDs and the specific molecular events underlying NLRP3 targeting within cells; evaluate their broad-spectrum efficacy and long-term in vivo biosafety in various models of bacterial and viral pneumonia, thereby laying the foundation for clinical translation; and further explore the therapeutic effects and mechanisms of different compound formulations against pneumonia.

Abbreviations

ALI, Acute lung injury; ALT, Alanine aminotransferase; ANOVA, One-way analysis of variance; AST, Aspartate aminotransferase; BCA, Bicinchoninic acid; BSA, Bovine serum albumin; BUN, Blood urea nitrogen; CDs, Carbon dots; CREA, Creatinine; dT, Dynabeads Oligo; ELISA, Enzyme-linked immunosorbent assay; ERK/MAPK, Extracellular signal-regulated kinase/mitogen-activated protein kinase; FC, Fold change; H&E, Hematoxylin and eosin; IAV, Influenza A virus; IFN-β, Interferon-β; IL-17A, Interleukin-17A; IL-6, Interleukin-6; NF-κB, Nuclear factor kappa B; NLRP3, NOD-, LRR-, and pyrin domain containing protein 3; NP, Nucleoprotein; Nrf2, Nuclear factor erythroid 2-related factor 2; PDE4, Phosphodiesterase 4; PolyA, Polyadenylated; PVDF, Polyvinylidene fluoride; QH-CDs, CDs co-derived from *Artemisia annua* and *Scutellaria baicalensis*; qRT-PCR, Quantitative real-time polymerase chain reaction; RIN, RNA integrity number; SDS-PAGE, Sodium dodecyl sulfate-polyacrylamide gel electrophoresis; TBST, Tris-Buffered Saline with Tween; $TCID_{50}$, 50% tissue culture infectious dose; TCM, Traditional Chinese medicine; TEM, Transmission electron microscopy; TGF-β, Transforming growth factor β; TLR4/p65, Toll-like receptor 4/RELA; TNF-α, Tumor necrosis factor-α; UV-Vis, Ultraviolet-visible; vRNP, Viral ribonucleoprotein; XRD, X-ray diffraction.

Ethics Approval and Consent to Participate

All the animal experiments were conducted in accordance with the institutional guidelines and approved by Institute of Basic Medicine and Oncology, Chinese Academy of Sciences Animal Experiments Ethical Inspection of Zhejiang Center of Laboratory Animals (2024R0120301). The experimental mice were euthanized by cervical dislocation following anesthesia with isoflurane to minimize suffering. All the procedures involving animals were conducted in accordance with the ethical policies and procedures approved by the Zhejiang Laboratory Animal Center of Hangzhou Medical College (Quality Certification No. SCXK (Zhe) 2021-0002) and Experimental Facilities Certification No. SYXK (Zhe) 2024-0009). All the experiments were performed following relevant institutional and national guidelines and regulations.

Acknowledgments

We acknowledge TopEdit LLC for the linguistic editing and proofreading during the preparation of this manuscript.

Funding

This research was supported by the National Natural Science Foundation of China (Grant No.: 82174272), the Zhejiang Provincial Natural Science Foundation of China (Grant No.: ZCLMS25H2703), and the Key projects of Jinhua Science and Technology Bureau (Grant No.: 2024-3-038, 2026-3-016).

Disclosure

The authors declare that the research was conducted without any commercial or financial relationships that could be construed as a potential conflict of interest.

References

1. Gauld N, Martin S, Sinclair O, Petousis-Harris H, Dumble F, Grant CC. Influences on pregnant women's and health care professionals' behaviour regarding maternal vaccinations: a qualitative interview study. *Vaccines*. 2022;10(1):76. doi:10.3390/vaccines10010076
2. Brody H. Influenza. *Nature*. 2019;573(7774):S49. doi:10.1038/d41586-019-02750-x
3. Herold S, Becker C, Ridge KM, Budinger GR. Influenza virus-induced lung injury: pathogenesis and implications for treatment. *Eur Respir J*. 2015;45(5):1463–1478. doi:10.1183/09031936.00186214
4. Tokimatsu I, Nasu M. Anti-influenza A viral drug--amantadine. *Nihon Rinsho*. 2000;58(11):2288–2292.
5. Doshi P, Heneghan C, Jefferson T. Oseltamivir for influenza. *Lancet*. 2016;387(10014):124. doi:10.1016/S0140-6736(15)01282-9
6. Shirley M. Baloxavir marboxil: a review in acute uncomplicated influenza. *Drugs*. 2020;80(11):1109–1118. doi:10.1007/s40265-020-01350-8
7. Shiraki K, Daikoku T. Favipiravir, an anti-influenza drug against life-threatening RNA virus infections. *Pharmacol Ther*. 2020;209:107512. doi:10.1016/j.pharmthera.2020.107512
8. Gao D, Niu M, Wei SZ, et al. Identification of a pharmacological biomarker for the bioassay-based quality control of a thirteen-component TCM formula (Lianhua Qingwen) used in treating influenza A virus (H1N1) infection. *Front Pharmacol*. 2020;11:746. doi:10.3389/fphar.2020.00746
9. Yang X, Long F, Jia W, et al. Artesunate inhibits PDE4 leading to intracellular cAMP accumulation, reduced ERK/MAPK signaling, and blockade of influenza A virus vRNP nuclear export. *Antiviral Res*. 2023;215:105635. doi:10.1016/j.antiviral.2023.105635
10. Zhou YJ, Zhang J, Wu B, Li Z, Wu J, Bie MJ. Therapeutic effect of artesunate on influenza A viral pneumonia. *Sichuan Da Xue Xue Bao Yi Xue Ban*. 2022;53(6):1055–1060. doi:10.12182/20221160205
11. Zhao X, Dai X, Wang F, et al. Artemisia annua L. leaf extracts suppress influenza virus infection by targeting the viral nucleoprotein and blocking mitochondria-mediated apoptosis. *Virol Sin*. 2025;40(2):247–259. doi:10.1016/j.virs.2025.03.001
12. Ye L, Gao Y, Mok SWF, et al. Modulation of alveolar macrophage and mitochondrial fitness by medicinal plant-derived nanovesicles to mitigate acute lung injury and viral pneumonia. *J Nanobiotechnol*. 2024;22(1):190. doi:10.1186/s12951-024-02473-w
13. Moghaddam E, Teoh BT, Sam SS, et al. Baicalin, a metabolite of baicalein with antiviral activity against dengue virus. *Sci Rep*. 2014;4(1):5452. doi:10.1038/srep05452
14. Low ZX, OuYong BM, Hassandarvish P, Poh CL, Ramanathan B. Antiviral activity of silymarin and baicalein against dengue virus. *Sci Rep*. 2021;11(1):21221. doi:10.1038/s41598-021-98949-y
15. Niu Q, Zhou C, Li R, et al. Proteomic analysis reveals the antiviral effects of baicalin on pseudorabies virus. *Int J Biol Macromol*. 2024;277:134149. doi:10.1016/j.ijbiomac.2024.134149
16. Dinda B, Dinda M, Dinda S, De UC. An overview of anti-SARS-CoV-2 and anti-inflammatory potential of baicalein and its metabolite baicalin: insights into molecular mechanisms. *Eur J Med Chem*. 2023;258:115629. doi:10.1016/j.ejmech.2023.115629
17. Lin CC, Shieh DE. The anti-inflammatory activity of scutellaria rivularis extracts and its active components, baicalin, baicalein and wogonin. *Am J Chin Med*. 1996;24(01):31–36. doi:10.1142/S0192415X96000050
18. Wang L, Huang S, Liang X, et al. Immuno-modulatory role of baicalin in atherosclerosis prevention and treatment: current scenario and future directions. *Front Immunol*. 2024;15:1377470. doi:10.3389/fimmu.2024.1377470
19. Shu X, Zhang Y, Zhang X, et al. Therapeutic and immune-regulation effects of Scutellaria baicalensis Georgi polysaccharide on pseudorabies in piglets. *Front Vet Sci*. 2024;11:1356819. doi:10.3389/fvets.2024.1356819
20. Ji S, Li R, Wang Q, et al. Anti-H1N1 virus, cytotoxic and Nrf2 activation activities of chemical constituents from Scutellaria baicalensis. *J Ethnopharmacol*. 2015;176:475–484. doi:10.1016/j.jep.2015.11.018
21. Zhang S, Xia J, Zhu Y, Dong M, Wang J. Establishing salvia miltiorrhiza-derived exosome-like nanoparticles and elucidating their role in angiogenesis. *Molecules*. 2024;29(7). doi:10.3390/molecules29071599
22. Qirong L, Zhang Y, Shi B, et al. Galangin exosomes induce cell apoptosis through miR-10b/P53 axis in gastric cancer. *Sci Rep*. 2025;15(1). doi:10.1038/s41598-025-95908-9
23. Zhang J, Zou L, Qinglong L, et al. Carbon dots derived from traditional Chinese medicines with bioactivities: a rising star in clinical treatment. *ACS Appl Bio Mater*. 2023;6(10):3984–4001. doi:10.1021/acsabm.3c00462
24. Han B, Shen L, Xie H, et al. Synthesis of carbon dots with hemostatic effects using traditional Chinese medicine as a biomass carbon source. *ACS Omega*. 2023;8(3):3176–3183. doi:10.1021/acsomega.2c06600
25. Li D, Xu KY, Zhao WP, et al. Chinese medicinal herb-derived carbon dots for common diseases: efficacies and potential mechanisms. *Front Pharmacol*. 2022;13:815479. doi:10.3389/fphar.2022.815479
26. Yang QQ, Jin JC, Xu ZQ, et al. Active site-targeted carbon dots for the inhibition of human insulin fibrillation. *J Mat Chem B*. 2017;5(10):2010–2018. doi:10.1039/c6tb02823c
27. Aiyer S, Prasad R, Kumar M, Nirvikar K, Jain B, Omkar SK. Fluorescent carbon nanodots for targeted in vitro cancer cell imaging. *Appl Mater Today*. 2016;4:71–77. doi:10.1016/j.apmt.2016.07.001
28. Tong T, Hu H, Zhou J, et al. Glycyrrhizic-acid-based carbon dots with high antiviral activity by multisite inhibition mechanisms. *Small*. 2020;16(13):e1906206. doi:10.1002/smll.201906206
29. Zhao Y, Cheng G, Gao Y, et al. Green synthetic natural carbon dots derived from Fuligo Plantae with inhibitory effect against alcoholic gastric ulcer. *Front Mol Biosci*. 2023;10:1223621. doi:10.3389/fmolb.2023.1223621
30. Kwon E-B, You-Chang O, Hwang Y-H, et al. A herbal mixture formula of OCD20015-V009 prophylactic administration to enhance interferon-mediated antiviral activity against influenza A virus. *Front Pharmacol*. 2021;12. doi:10.3389/fphar.2021.764297
31. Qinhai M, Qingtian Y, Xing X, Liu S, Shi C, Luo J. San wu huangqin decoction, a Chinese herbal formula, inhibits influenza a/PR/8/34 (H1N1) virus infection in vitro and in vivo. *Viruses*. 2018;10(3). doi:10.3390/v10030117

32. De Faveri Favero F, Basting RT, de Freitas AS, et al. Artemisinin and deoxyartemisinin isolated from Artemisia annua L. promote distinct antinociceptive and anti-inflammatory effects in an animal model. *Biomed Pharmacother*. 2024;178. doi:10.1016/j.biopha.2024.117299
33. Wang M, Yang Y, Changqiang K, et al. Sesquiterpene lactones from Artemisia verlotorum and their anti-inflammatory activities. *Fitoterapia*. 2023;169:105560. doi:10.1016/j.fitote.2023.105560
34. Liu H, Zhen L, Zhang Y, et al. Antiviral effects of artemisinin and its derivatives. *Chin Med J*. 2023;136(24):2993–2995. doi:10.1097/cm9.0000000000002934
35. Baggieri M, Gioacchini S, Borgonovo G, et al. Antiviral, virucidal and antioxidant properties of Artemisia annua against SARS-CoV-2. *Biomed Pharmacother*. 2023;168:115682. doi:10.1016/j.biopha.2023.115682
36. Liu X-Y, Xie W, Zhou H-Y, Zhang H-Q, Jin Y-S. A comprehensive overview on antiviral effects of baicalein and its glucuronide derivative baicalin. *J Integr Med*. 2024;22(6):621–636. doi:10.1016/j.joim.2024.09.003
37. Qiu C, Zhang JZ, Wu B, et al. Advanced application of nanotechnology in active constituents of traditional Chinese medicines. *J Nanobiotechnol*. 2023;21(1). doi:10.1186/s12951-023-02165-x
38. Zhang Y-B, Wang J-F, Wang M-X, Peng J, Kong X-D, Tian J. Frontiers | nano-based drug delivery systems for active ingredients from traditional Chinese medicine: harnessing the power of nanotechnology. *Front Pharmacol*. 2024;15. doi:10.3389/fphar.2024.1405252
39. Qiao L, Lianghao Y, Shijie G, et al. Self-assembled nanodrug delivery systems for anti-cancer drugs from traditional Chinese medicine. *Biomater Sci*. 2024;12(7):1662–1692. doi:10.1039/d3bm01451g
40. Wang J, Li LL, Zhao ZA, Niu CY, Zhao ZG. NLRP3 Inflammasome-mediated pyroptosis in acute lung injury: roles of main lung cell types and therapeutic perspectives. *Int Immunopharmacol*. 2025;154:114560. doi:10.1016/j.intimp.2025.114560
41. Chen A, Yanmin W, Jun W, et al. Berberine ameliorates pulmonary inflammation in mice with influenza viral pneumonia by inhibiting NLRP3 inflammasome activation and gasdermin D-mediated pyroptosis. *Drug Dev Res*. 2022;83(7):1707–1721. doi:10.1002/ddr.21995